Orbit Determination Strategy and Accuracy for a Comet Rendezvous Mission

James K. Miller*
Jet Propulsion Laboratory, California Institute of Technology, Pasadena, California
Connie J. Weeks†
Loyola Marymount University, Los Angeles, California
Lincoln J. Wood‡
Jet Propulsion Laboratory, California Institute of Technology, Pasadena, California

Orbit determination during the postrendezvous phases of the Comet Rendezvous/Asteroid Flyby mission is described. The orbit determination process is discussed, with emphasis placed on optical imaging of landmarks, Doppler tracking, and the effects of nongravitational accelerations. Rotational dynamics are introduced for the cometary nucleus. State estimation errors are given for spacecraft trajectory prediction and cometary nucleus attitude prediction. Estimation errors are also given for physical parameters that describe the cometary nucleus such as moments of inertia and gravity field harmonics. The orbit determination performance in support of science instrument pointing while in orbit about the nucleus is described.

Introduction

THE Comet Rendezvous/Asteroid Flyby mission is the first of a series of missions using the Mariner Mark II spacecraft planned for the 1990s and thereafter.[1,2] The primary purpose of this mission is to orbit the nucleus of a periodic comet and to study it at close range. A secondary purpose is to fly by and observe an asteroid en route to the comet. The Mariner Mark II spacecraft is launched on a trajectory that intercepts the target comet (presently Kopff) near aphelion. A large motor burn places the spacecraft in a distant rendezvous orbit with the comet. After a series of approach maneuvers, the spacecraft is placed in a closed orbit about the cometary nucleus beginning what we refer to as the orbit phase of the mission.

Previous analyses of the orbit phase have assumed a relatively simple model for the cometary nucleus consisting of a spherically symmetric mass distribution or a cluster of point masses rotating at a uniform rate with the spin vector fixed in inertial space.[3,4] Optical imaging of the nucleus was limited to locating the optical center of the nucleus on a star background. This study makes use of a more refined model of the nucleus. The modeled nucleus now consists of a central body that is described by gravity harmonics and is covered with a number of point masses called mascons and a number of identifiable surface landmark features. Rotational dynamics are introduced, and the rotational mass properties are described by an inertia tensor. Outgassing from the surface is described by simple models of force on the spacecraft and reaction torques on the nucleus. The dynamics of the spacecraft and cometary nucleus are obtained by integrating the spacecraft translational equations of motion in conjunction with the rotational equations of motion for the cometary nucleus.

The orbit determination strategy and the resulting accuracies are discussed for various combinations of data types, model parameter errors, and orbital geometries. The data types include Doppler, range, differential very long baseline interferometry (ΔVLBI), and optical imaging of the cometary nucleus. Of particular interest is the modeling of the optical imaging data type. In previous missions, the imaged objects have been large and nearly spherical and have been observed from relatively large distances. A cometary nucleus is expected to be highly irregular in shape and will be observed from several tens of kilometers. At this distance, it will be difficult to consistently locate a point in three dimensions that defines the center of figure when observations of only the lit limb and terminator, or portions thereof, are available. An alternative technique is to image a set of fixed landmarks on the surface of the nucleus and to determine the orbit of the spacecraft directly by tracking these landmarks. Since the location of the landmarks in inertial space is dependent on the attitude of the nucleus, the orbit determination involves a joint solution for cometary nucleus attitude, landmark locations, and spacecraft position and velocity, as well as other dynamic parameters including nongravitational accelerations and gravity model parameters.

Because of the expected irregular shape and weak gravity field, the gravity field determination presents a challenging problem. In a previous analysis,[4] the gravity potential was modeled in terms of a cluster of five mass concentrations (mascons) with the largest at the center and the other four at the corners of a tetrahedron. This model could be made to represent, at least very roughly, all sizes and shapes that one may expect to find by adjusting the masses of the mascons. In this paper, a somewhat different approach is taken. The gross shape is modeled as an ellipsoid with several mascons placed on the surface and the resulting gravity field is approximated by an appropriate low-order set of Legendre polynomials.

A problem with the determination of the orbit of a spacecraft about a cometary nucleus is the relatively large effect of nongravitational accelerations. These spacecraft accelerations are due to attitude control gas leaks, solar radiation pressure, and outgassing from the nucleus. The latter effect acts on the spacecraft and cometary nucleus to produce both translational and rotational accelerations. Since the nongravitational forces and torques vary somewhat unpredictably with time, a stochastic error model is developed.

Presented as Paper 89-0348 at the AIAA 27th Aerospace Sciences Meeting, Reno, NV, Jan. 9-12, 1989; received March 20, 1989; revision received Feb. 8, 1990. Copyright © 1989 by the American Institute of Aeronautics and Astronautics, Inc. All rights reserved.

*Member of the Technical Staff, Navigation Systems Section. Member AIAA.
†Assistant Professor, Department of Mathematics.
‡Technical Manager, Navigation Systems Section. Associate Fellow AIAA.

Physical Model of the Cometary Nucleus

Determination of the orbit of a spacecraft about a cometary nucleus is intimately associated with development of an accurate model of the nucleus. The cometary nucleus is the principal source of perturbations of the spacecraft's trajectory and the principal source of data for determining the orbit. The cometary nucleus affects the spacecraft motion in two ways. The gravitational field results in a force that accelerates the spacecraft toward the nucleus, and the solar energy input results in a stream of dust and gas molecules that accelerates the spacecraft away from the nucleus. The reaction force associated with the momentum imparted to dust and gas molecules also results in rotational and translational accelerations of the nucleus. One other characteristic of the nucleus that is important for orbit determination is the existence of landmarks on the surface. To be useful for orbit determination, the landmarks must be readily identifiable in images taken from different slant ranges and under a variety of lighting conditions. The existence of landmarks implies a surface that is varied in detail with some recognizable pattern, as would be caused by cratering or fracturing, for example. All the bodies in the solar system whose surfaces have been observed contain an abundant supply of surface features that may be used as landmarks for orbit determination, and it is expected that a cometary nucleus will have an adequate supply.

The model of the cometary nucleus used for orbit determination is similar to the model used by the project science team. The major difference is in emphasis of detail. In addition, the parameters of the orbit determination model have been biased slightly for conservatism. The details of the model of the nucleus used for orbit determination studies are given in Table 1. The shape is assumed to be a prolate ellipsoid of revolution with the semimajor axis twice as long as the semiminor axes. The volume is equal to the volume of a sphere 3 km in radius, and the mass is equal to that of the same volume composed of water ice. (The current scientific model is somewhat larger and less dense.) For rotational stability, the polar axis, or z axis, is perpendicular to the long axis. The long axis is therefore in the equatorial plane and is taken to be the x axis. Longitude (body centered) is measured positive east from the x axis. Since the prolate ellipsoid is assumed circularly symmetric about its long axis, the moments of inertia about any transverse axes through the center of mass are equal. To further define the inertia tensor and enrich the gravity harmonic content, four mascons are placed in the equatorial plane. These are placed between the x and y axes at a radius of 3 km and contain in total 25% of the mass of the nucleus. Four landmarks are distributed over the nucleus such that at least two are always visible when the nucleus is viewed from any direction.

Table 1 Physical model of cometary nucleus

Parameters	Values			
Shape	prolate ellipsoid			
Semi x axis, km	4.76			
Semi y axis, km	2.38			
Semi z axis, km	2.38			
Landmark locations				
Landmark number	1	2	3	4
Longitude, deg	45	135	225	315
Latitude, deg	45	−45	−45	45
Radius, km	3.84	3.84	3.84	3.84
Mascons				
Mascon number	1	2	3	4
Longitude, deg	45	135	225	315
Latitude, deg	0	0	0	0
Radius, km	3	3	3	3
Mass, kg	7.1×10^{12}	7.1×10^{12}	7.1×10^{12}	7.1×10^{12}
Mass, kg				
Prolate ellipsoid	8.48×10^{13}			
Mascon masses	2.82×10^{13}			
Total mass	1.13×10^{14}			
Gravity harmonics				
μ, km^3/s^2	7.52×10^{-6}			
C_{20}, C_{22}	−0.500	+0.140		
C_{40}, C_{42}, C_{44}	+0.053	−0.032	+0.00070	
C_{60}, C_{62}, C_{64}, C_{66}	−0.072	+0.021	−0.00014	+0.000056
Moments of inertia, kg-m^2				
I_{xx}, I_{yy}, I_{zz}	3.9×10^{20}	7.7×10^{20}	8.9×10^{20}	
I_{xy}, I_{xz}, I_{yz}	0	0	0	
Outgassing				
Mass flux, kg/m^2-s	9.3×10^{-8}			
Velocity, m/s	800			
Active area, m^2	1.0×10^{6}			
Moment arm, m	2.0×10^{3}			
M_x, M_y, M_z, N-m	1.4×10^{5}	1.4×10^{5}	1.4×10^{5}	

The solar energy input results in a heating rate of the nucleus that attains a peak at the subsolar point. This heat input is mostly reradiated to space, but a substantial fraction results in sublimation of the water ice that is assumed to constitute the bulk of the cometary nucleus.[5] The stream of gas molecules emanating from the surface imparts a reaction torque to the nucleus. The outgassing moment given in Table 1 assumes a nucleus at 4.6 a.u. from the sun, where the outgassing mass flux at the surface is estimated to be 9.3×10^{-8} kg/s-m^2. The gas molecules are assumed to leave the surface with an average velocity of 800 m/s over an active area of 1 km^2 with an effective moment arm of 2 km.

The remaining parameters given in Table 1 are derived from the aforementioned data. The gravity harmonics are obtained by integrating the coefficient generating function over the enclosed volume assuming constant density and adding the harmonic coefficients associated with the mascons. The moments of inertia are also obtained by integration over the same mass distribution.

Spacecraft Nongravitational Accelerations

For an orbiting spacecraft, the orbit determination error is a function of errors associated with the measurement system and errors associated with modeling the dynamics of the spacecraft motion. Spacecraft dynamics are the direct result of forces acting on the spacecraft. These forces may be separated into two categories: gravitational forces arising from the central body and other bodies in the solar system, and nongravitational forces arising from a variety of sources including solar radiation pressure, impinging dust particles and gas molecules from the nucleus, and attitude control system gas leaks or thruster imbalance. Both the gravitational and nongravitational forces accelerate the spacecraft; however, only the nongravitational accelerations may be detected by an accelerometer. The gravitational accelerations are determined by observing the motion of the spacecraft and, in the absence of a sufficiently sensitive accelerometer, the nongravitational accelerations are determined the same way. The determination of the spacecraft orbit is thus dependent on the development of accurate models of the gravity field and the nongravitational force environment. The gravity field is generally easier to model in structural terms than nongravitational forces; however, the nongravitational forces are several orders of magnitude smaller. In general, the stronger the gravitational forces and the weaker the nongravitational forces, the easier it is to determine the orbit.

Nongravitational accelerations that are constant may be modeled as bias parameters and are relatively easy to determine. Rapidly varying nongravitational accelerations tend to statistically average out over time. The most troublesome nongravitational accelerations are time varying at frequencies commensurate with the orbit period or the length of the data arc. The assumed a priori nongravitational accelerations associated with outgassing, attitude control gas leaks, and solar pressure are given in Table 2. These have been separated into

constant and variable modeling error components. The constant component is simply the average acceleration modeling error, and the variable component is the assumed error in the acceleration model that varies as a function of time. The acceleration due to dust and gas is computed from the data given in Table 1, evaluated at the subsolar point of the nucleus.

Radiometric Data

Radiometric tracking data provide observations of the spacecraft motion with respect to the stations that comprise the Deep Space Network (DSN). The DSN tracking stations transmit radio-frequency signals to the spacecraft and receive signals via the spacecraft transponder and antenna. The received signals constitute observations of Doppler, range, and ΔVLBI data. Doppler data provide a direct measure of line-of-sight velocity of a spacecraft relative to the tracking antenna. The accuracy of this measurement is about 1 mm/s at S-band frequencies and 0.1 mm/s at X-band frequencies when the two-way Doppler count is integrated for 1 min. A single Doppler measurement provides no information on position and velocity normal to the line of sight; however, a series of Doppler measurements enables a precise determination of certain orbit parameters by observing the signatures due to the Earth's rotation[6] and orbit dynamics in the data. The size, shape, and period of the orbit are well determined, provided the gravity field of the central body is known, and the orientation is marginally determined.[7]

Range data provide a direct measure of the line-of-sight distance from an Earth tracking station to the spacecraft. The absolute range measurement is useful for determining the cometary ephemeris, but is only marginally useful for determining the orbit of the spacecraft relative to the nucleus. For determination of the spacecraft orbit, the difference of successive range measurements is more directly useful. Differenced range may be obtained by differencing two range measurements taken over an interval of time or by integrating the Doppler data over the same interval. Since the integrated Doppler data are more accurate, this data type is used as the primary source of this information. However, the range data type provides the constant of integration that is needed for determination of the comet's orbit relative to the sun. Ranging

Table 2 Spacecraft nongravitational accelerations

Parameters	Values
Mass	1500 kg
Dust and gas pressure	
Effective area	12 m^2
Momentum transfer coefficient	1.5
Acceleration, 25-km orbit	
Constant bias, km/s^2	8.5×10^{-12}
Variable modeling error, km/s^2	8.5×10^{-13}
Attitude control gas leaks	
Acceleration	
Constant bias, km/s^2	5.0×10^{-12}
Variable modeling error, km/s^2	5.0×10^{-13}
Solar pressure	
Effective area	12 m^2
Momentum transfer coefficient	1.5
Acceleration	
Constant bias, km/s^2	2.6×10^{-12}
Variable modeling error, km/s^2	2.6×10^{-13}

Table 3 Orbit determination model errors

Parameters	Errors, 1σ
Data noise	
X-band Doppler	0.1 mm/s
X-band range	1 km
Optical imaging	
Lines	20 m (at nucleus surface)
Pixels	20 m (at nucleus surface)
Estimated parameters (a priori)	
Spacecraft	
Position	∞
Velocity	∞
Constant acceleration	5.0×10^{-12} km/s^2
Stochastic acceleration	
1-day correlation time	5.0×10^{-13} km/s^2
5-day correlation time	5.0×10^{-13} km/s^2
Comet	
Position	10,000 km
Velocity	1.0 km/s
Gravity harmonic coefficients	
μ	7.52×10^{-6} km^3/s^2
C_{20}, C_{21}, C_{22}	1.0 1.0 1.0
S_{21}, S_{22}	1.0 1.0
C_{30}, C_{31}, C_{32}, C_{33}	1.0 1.0 1.0 1.0
S_{31}, S_{32}, S_{33}	1.0 1.0 1.0
Attitude	
Orientation angles	20 deg
Angular rates	20 deg/s
Moments of inertia	∞
Applied moments	∞
Landmark locations	200 m
Considered parameters	
Station locations	
Spin radius	0.5 m
Longitude	0.5 m
z height	10 m
Comet	
Gravity harmonic coefficients	
C_{40}, C_{41}, C_{42}, C_{43}, C_{44}	0.5, 0.0315, 0.0267, 0.00524, 0.00262
S_{41}, S_{42}, S_{43}, S_{44}	0.0315, 0.0267, 0.00524, 0.00262

data are weighted as though they are accurate to 1 km, although the real accuracy is substantially better than this.

ΔVLBI data provide an accurate determination of spacecraft right ascension and declination in the plane-of-the-sky coordinate system. However, for the geocentric distances and the orbit sizes with which we are concerned, this data type has limited effectiveness, at current accuracies, for determining the motion of the spacecraft about the cometary nucleus. The ΔVLBI data type is still a part of the orbit determination strategy and may prove useful for reducing the amount of Doppler tracking coverage.

Landmark Tracking

Optical imaging of the cometary nucleus provides a powerful data type for aiding in the determination of the spacecraft orbit and describing certain characteristics of the cometary nucleus. Optical data alone are insufficient for complete orbit determination but are an essential complement to the Doppler data. When optical data are combined with Doppler data, an accurate determination of orbit orientation, size, and shape is obtained.

The optical measurement is obtained from an image of the cometary nucleus on a star background. At a minimum, the angle between the star and a point on the cometary nucleus can be obtained. If there is more than one star in the imaging frame, or the twist angle about the line of sight is known from an independent determination of spacecraft attitude, the right ascension and declination relative to the spacecraft of any discernible landmark on the cometary nucleus can be determined. The accuracy of this data type is a function of the picture element (pixel) spacing and the focal length of the camera optics. For a narrow angle camera with a focal length of 2000 mm and pixel spacing of 70 pixels/mm, one pixel resolution translates into a 7.14 μrad angular measurement error. At a range of 20 km, the position resolution normal to the line of sight is less than 1 m. Previous flight experience has indicated that landmarks may be identified and located to an accuracy of about 1 pixel, for a pixel size of several hundred meters. To achieve this accuracy, the landmark must be identified as a unique surface feature by correlation with other surface features. This correlation may be performed by the human eye or perhaps by a computer program. At a scale of less than 1 m, it is assumed that the identification and location of landmarks may require several pixels of resolution. To be conservative, the pixel measurement error in the analysis that follows was adjusted to give a 20-m position measurement error at the surface of the nucleus.

Error Model

The study of orbit determination involves the development of models describing the spacecraft, the physical environment, and the instrumentation and data acquisition associated with orbit determination. These models are generally not worst case but represent a reasonable reproduction of the system being investigated. Conservatism, if any, is introduced by assigning a priori errors that may be a little larger than their estimated values or by restricting the data set to a smaller number of observations than are available. The orbit determination study consists of computer simulations of a large number of cases varying the important system parameters. However, since only a limited amount of information has been gathered on the physical characteristics of cometary nuclei, the model that has been studied is probably considerably different from the actual nucleus that will be encountered by the Mariner Mark II spacecraft. Therefore, the values of the parameters in this model have been biased slightly toward conservatism, but not far enough to be unrealistic.

The errors associated with the parameters of the orbit determination model are given in Table 3. These are separated into data noise errors, a priori errors in the estimated parameters, and errors in the considered parameters. The data noise errors have already been discussed. The estimated parameters are those parameters that are included in the orbit determination solution, and the a priori error is the initial error resulting from previous estimates of these parameters or other sources of information. In general, the a priori errors in the estimated parameters are set to very large values provided there is sufficient strength in the data to determine these parameters. A notable exception is the nongravitational accelerations of the spacecraft. These include dust and outgassing effects, attitude control gas leaks, and solar radiation pressure. The nongravitational accelerations are lumped together as a constant acceleration and as stochastic accelerations. The stochastic accelerations are separated into two components and modeled as exponentially correlated process noise with correlation times of 1 day and 5 days, respectively.

Some parameters cannot be modeled with sufficient precision to be estimated, and the systematic errors associated with these parameters are considered by the filter.[8] The considered parameters are DSN station locations and some of the high-order gravity harmonic coefficients. The sensitivity of the filter to considered parameters places a lower limit on the orbit determination accuracy. Of particular interest is the truncation error associated with the terms of the gravity field expansion that are not estimated. The worst-case truncation error occurs for a worst-case distribution of the nucleus mass. It can be shown that the worst-case mass distribution of a body whose maximum radius is known is two point masses arranged like a dumbbell. For this distribution, the coefficients of the even Legendre polynomials are unity, and the odd coefficients are zero. However, this mass distribution is rather extreme, and a more reasonable "worst" case is taken to be a rod of uniform density. The coefficients of the Legendre polynomials for a rod are

$$C_{n0} = \begin{cases} \dfrac{1}{(n+1)} & \text{for } n \text{ even} \\ 0 & \text{for } n \text{ odd} \end{cases}$$

Table 4 Initial conditions

Parameters	Values
Initial epoch	June 28, 1997
Spacecraft ephemeris	Comet-centered plane-of-the sky frame
$X_0 = \begin{bmatrix} r_{p_0} \\ e_0 \\ \Omega_0 \\ i_0 \\ \omega_0 \end{bmatrix}$	$X_0 = \begin{bmatrix} 20\text{ km} \\ 0.05 \\ 45\text{ deg} \\ 45\text{ deg} \\ 0\text{ deg} \end{bmatrix}$
Comet ephemeris	Sun-centered EME50 frame
$X_c = \begin{bmatrix} x_c \\ y_c \\ z_c \\ v_{xc} \\ v_{yc} \\ v_{zc} \end{bmatrix}$	$X_c = \begin{bmatrix} -5.62\times10^8\text{ km} \\ +3.30\times10^8\text{ km} \\ +2.16\times10^8\text{ km} \\ -3.34\text{ km/s} \\ -9.17\text{ km/s} \\ -2.29\text{ km/s} \end{bmatrix}$
Comet attitude and rates	Rotations from EME50 frame
$\Phi_0 = \begin{bmatrix} \alpha_0 \\ \delta_0 \\ \theta_0 \\ \Delta_{50} \\ \omega_{x0} \\ \omega_{y0} \\ \omega_{z0} \end{bmatrix}$	$\Phi_0 = \begin{bmatrix} 0\text{ deg} \\ 45\text{ deg} \\ 0\text{ deg} \\ 0\text{ deg} \\ 1.077\times10^{-4}\text{ rad/s} \\ 1.077\times10^{-4}\text{ rad/s} \\ 8.725\times10^{-3}\text{ rad/s} \end{bmatrix}$

The truncation error is simply the difference between the true gravity potential of a rod and the sum of the first i^* terms of the harmonic expansion. The maximum acceleration error is obtained by taking the gradient of the potential and is given by

$$\epsilon_a \leq \mu\left\{\frac{1}{2r_0(r-r_0)} - \frac{1}{2r_0(r+r_0)} - \sum_{i=0}^{i^*}\left(\frac{r_0^{2i}}{r^{2i+2}}\right)\right\} \quad (1)$$

For a spacecraft orbit radius r of 20 km and cometary nucleus radius r_0 of 3 km, we may compute the degree of the harmonic expansion i^* that yields an acceleration error ϵ_a less than the sensitivity threshold of the orbit determination process. This threshold is about 1×10^{-12} km/s^2, which gives a fourth-degree expansion. The gravity harmonic coefficients are estimated through degree and order three, and the fourth-degree harmonic coefficients are considered as a systematic error that represents the truncation error. The errors given in Table 3 are obtained by assuming rod-shaped distributions along the coordinate axes.

Nominal Orbit Profile

During the orbit phase, the spacecraft is maneuvered into many different orbits to satisfy mission objectives. Previous studies, which assume that both radio and optical data are available, have shown that orbit determination errors are relatively insensitive to orbit parameters with the exception of the size or period of the orbit. In this study, variations in orbit size were produced by varying the periapsis radius, with eccentricity held constant. The initial conditions for a 20-km orbit are given in Table 4. Orbit elements are given in comet-centered, plane-of-sky coordinates. This orbit is nearly circular and inclined at 45 deg to avoid singularities associated with Doppler data. The orbit elements given in Table 4 describe only the initial spacecraft state. These initial conditions are propagated by numerical integration that includes the central-body gravity, the perturbative accelerations of the nucleus gravity harmonics and the sun, and nongravitational accelerations. The spacecraft is in a fairly tightly bound orbit about the nucleus, and over 30 days the orbit elements change only a small amount due to the various perturbing forces.

Also shown in Table 4 are the cometary ephemeris and initial attitude. The cometary ephemeris is that of the periodic comet Tempel 2. At the initial distance of 4.6 a.u. from the sun, the comet is relatively inactive. Since the orbit of the comet has relatively little effect on spacecraft orbit determination accuracy, the orbit of Tempel 2 was selected for convenience (even though it is no longer the planned cometary target).

The conventional method of describing the attitude of a rotating body is a set of Euler angles. The Euler angles define consecutive rotations about body-fixed axes that transform a vector from an inertial reference frame to body-fixed axes. A problem with Euler angles is that the transformation of Euler angle rates to rotations about body-fixed axes is singular for certain attitudes. These singular attitudes may be avoided by switching to an alternate set of Euler angles when near a singular attitude. Another approach is to describe the attitude by a set of Cayley-Klein parameters or quaternions,[9] which would have the additional numerical advantage of maintaining an accurate transformation matrix when the rotational equations of motion are integrated over many revolutions of the nucleus.

The inertial reference frame is defined by the Earth mean equator and equinox of 1950.0 with the z axis in the direction of Earth's north pole, the x axis in the direction of the vernal equinox, and the y axis completing the right-hand coordinate system. The attitude of the nucleus is described by the Euler angles right ascension α, declination δ, autumnal equinox Δ_{50}, and prime meridian θ. This set of angles is used by astronomers to define the inertial attitudes of the planets. The first rotation is a right-hand rotation about the inertial Earth mean equator and equinox of 1950.0 z axis through the right ascension angle α. The second rotation is a left-hand rotation about the y axis through the declination angle δ followed by a 90-deg right-hand rotation about the same axis to place the z axis in the direction of the north pole. The third rotation is a right-hand rotation about the z axis of 90 deg to place the x axis at the ascending node of the comet equator on the mean 1950.0 Earth equator followed by an additional rotation through the angle Δ_{50} to the autumnal equinox. The fourth and final rotation is another right-hand rotation about the z axis through the prime meridian angle θ. The angle Δ_{50} is defined at some reference epoch and held constant for the duration of the integration of Euler's equations. The autumnal equinox angle is combined with the prime meridian angle for convenience, and they may be separated when the integration of Euler's equations is complete.

The body-fixed spin rate is offset from the z axis or polar axis by 1 deg to induce nutation in the rotational motion of the nucleus. A free body rotating in inertial space will eventually settle down to a minimum energy state spinning about the axis of maximum moment of inertia. The possibility of neutrally stable rotation about the axis of minimum moment of inertia is discounted. Any external torque that induces a deviation from this state will cause the nucleus to nutate or rotate about some axis other than a principal axis. Nutation may also be induced by shape changes resulting from loss of material from the nucleus. A free body rotating about some axis other than a principal axis will dissipate energy through stress and strain hysteresis. The greater the nutation angle is, the greater the energy dissipation rate. As a consequence, the nucleus may be expected to decay exponentially to the minimum energy condition. Over many apparitions of a comet, a quasisteady-state nutation may be expected where the nutation induced by outgassing or a change of shape during perihelion passage is balanced by the stress and strain energy dissipation during the quiescent portions of the orbit. Thus, the nucleus may be expected to rotate about an axis that is roughly aligned with the principal axis of maximum moment of inertia.

Spacecraft Orbit Prediction

A detailed covariance analysis was performed to determine the predicted spacecraft orbit determination error at various epochs with respect to the end of the data arc (the time at which the last data point is acquired). Computer simulations of data scheduling, trajectory propagation, data filtering, and solution mapping were generated. The data arc spanned 30 days and included a continuous pattern of Doppler and range radio metric tracking data and optical images of the cometary nucleus. Radio metric data were taken from Deep Space Stations 14, 43, and 63, located at Goldstone, California; Canberra, Australia; and Madrid, Spain, respectively. The Doppler data were compressed to 1 point/h, and a single range

Table 5 Orbit determination sensitivity to Doppler measurement errors

	Sensitivities of errors in estimated parameters to errors in Doppler data, 20-km orbit		
Estimated parameter	Error source		
	$\dot{\rho}$	r_e	λ_e
r, m	$\frac{2\mu}{v^3 \sin i}\sigma_{\dot{\rho}}$	$\frac{2\mu\omega \sin\lambda_e}{v^3 \sin i \sec\delta_c}\sigma_{r_e}$	$\frac{2\mu\omega r_e \cos\lambda_e}{v^3 \sin i \sec\delta_c}\sigma_{\lambda_e}$
	1.19	$3.35 \sin\lambda_e$	$3.35 \cos\lambda_e$
v, mm/s	$\frac{1}{\sin i}\sigma_{\dot{\rho}}$	$\frac{\omega \sin\lambda_e}{\sin i \sec\delta_c}\sigma_{r_e}$	$\frac{\omega r_e \cos\lambda_e}{\sin i \sec\delta_c}\sigma_{\lambda_e}$
	0.018	$0.051 \sin\lambda_e$	$0.051 \cos\lambda_e$
μ, km^3/s^2	$\frac{2vr}{\sin i}\sigma_{\dot{\rho}}$	$\frac{2vr\omega \sin\lambda_e}{\sin i \sec\delta_c}\sigma_{r_e}$	$\frac{2vr\omega r_e \cos\lambda_e}{\sin i \sec\delta_c}\sigma_{\lambda_e}$
	4.47×10^{-10}	$1.26 \times 10^{-9} \times \sin\lambda_e$	$1.26 \times 10^{-9} \times \cos\lambda_e$

Table 6 Spacecraft orbit prediction errors

Prediction epoch[a]	Radial, m	Downtrack, m	Crosstrack, m
20-km orbit			
0 days	9.4	5.7	3.2
1 day	8.5	20.1	3.5
9 days	34.0	148	5.4
30-km orbit			
0 days	8.8	12.3	5.6
1 day	9.1	34.4	4.9
9 days	49.1	222	8.2
50-km orbit			
0 days	13.2	16.6	10.9
1 day	17.8	32.6	11.9
9 days	107.0	384	22.9
100-km orbit			
0 days	48.8	21.5	26.5
1 day	53.0	31.9	35.8
9 days	52.1	140	21.1
1500-km orbit			
0 days	2075	247	805
1 day	2147	262	861
9 days	3209	419	1,357

[a]Time from last data point used in solution.

point was taken from each station pass. The optical data rate was 1 frame every 3 h. The simulated data were processed by a square-root information filter.

To obtain an estimate of the strength of Doppler data in determining the orbit of a spacecraft about a distant body, consider the following simplified example. For a distant spacecraft in a circular orbit about a cometary nucleus, the Doppler measurement is given by

$$\dot{\rho} = v_c + v \sin i \cos(\omega_s t + \theta_s) - \omega_e r_e \cos\delta_c \sin(\omega_e t + \lambda_e) \tag{2}$$

where v is the magnitude of the velocity relative to the nucleus and i is the inclination of the orbit in the plane-of-the-sky coordinate system. The orbital rotation rate, or mean motion, of the spacecraft about the nucleus is given by ω_s and θ_s is the angle measured from the crossing of the ascending node in the plane of the sky to the spacecraft at the initial time. The Earth-based tracking station is at longitude λ_e and distance off the spin axis r_e, and ω_e is the Earth's rotation rate. The cometary nucleus is at declination angle δ_c relative to the Earth, and the Earth-relative velocity component of the nucleus along the line of sight is given by v_c. For a circular orbit of radius r and a cometary nucleus with gravitational parameter μ, the magnitude of the velocity is given by

$$v = \sqrt{\mu/r} \tag{3}$$

The sensitivities of spacecraft orbit determination and cometary nucleus gravity estimation to errors in the Doppler measurement system based on the preceding model are given in Table 5. This simplified analysis assumes that 60 Doppler measurements taken over 1 h are compressed to a single Doppler data point at the nodal crossing. A more accurate treatment of the information content in Doppler data derived from an orbiting spacecraft is much more complicated and is presented in Ref. 7. The total error is simply the root sum square of the individual error components given in the table. The numerical values were computed for a spacecraft in a 20-km circular orbit with inclination in the plane of the sky equal to 45 deg. This analysis ignores cometary ephemeris errors, nongravitational accelerations, and many other error sources that are included in a complete analysis. We have implicitly assumed that optical data are available to determine the inclination and orientation of the orbit in the plane of the sky. The spacecraft orbit determination error associated with optical imaging is a reflection of the surface measurement error and is therefore roughly 20 m.

Having deduced very rough values of orbit determination uncertainties based on simple approximations, we now describe the results of the detailed covariance studies. The spacecraft orbit determination errors are described in an orthogonal rotating frame with the x_s axis directed radially from the center of the cometary nucleus to the spacecraft (the *radial* direction), the y_s axis normal to the radial direction and in the plane of motion (the *downtrack* direction), and the z_s axis normal to the plane of motion (the *crosstrack* direction). For a circular orbit, the downtrack direction is along the velocity vector. Orbit determination results are shown in Table 6 for orbits with various periapsis radii ranging from 20 to 1500 km. The orbits are nearly circular with elements other than periapsis radius given in Table 4. The radial, downtrack, and crosstrack orbit determination errors are given for orbit prediction times of 0, 1, and 9 days. These values are generally consistent with the preceding simplified analysis. The orbit determination errors grow monotonically in semimajor axis of the error ellipsoid as the prediction time increases. Some individual components may decrease with time due to variations in the mapped true anomaly. The orbit determination errors also tend to increase as the radius of the orbit is increased, presumably due to the decreasing strength of the Doppler data.

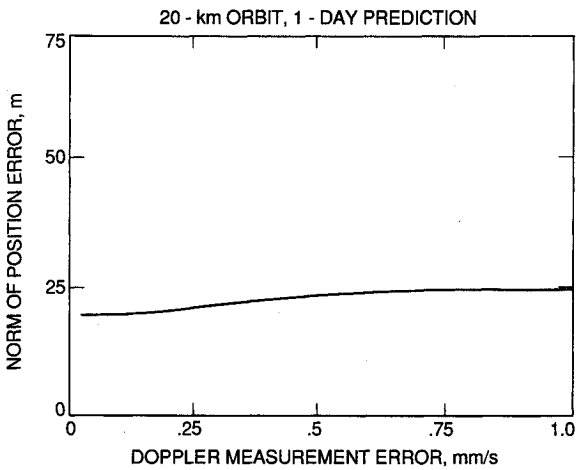

Fig. 1 Spacecraft orbit prediction error as function of Doppler measurement error.

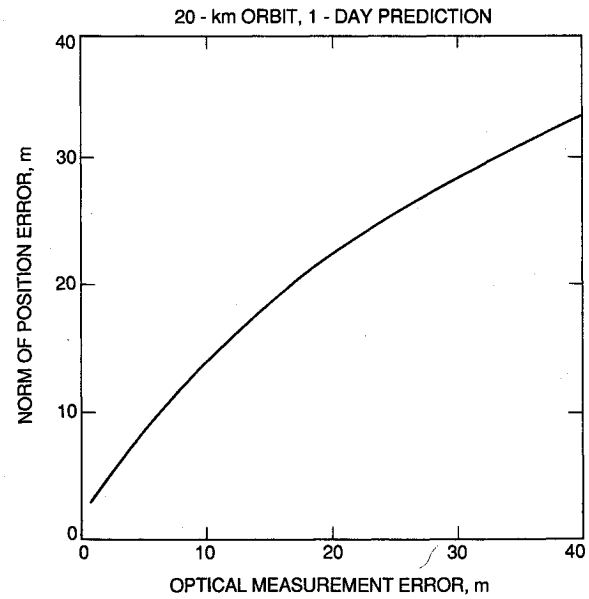

Fig. 2 Spacecraft orbit prediction error as function of optical measurement error.

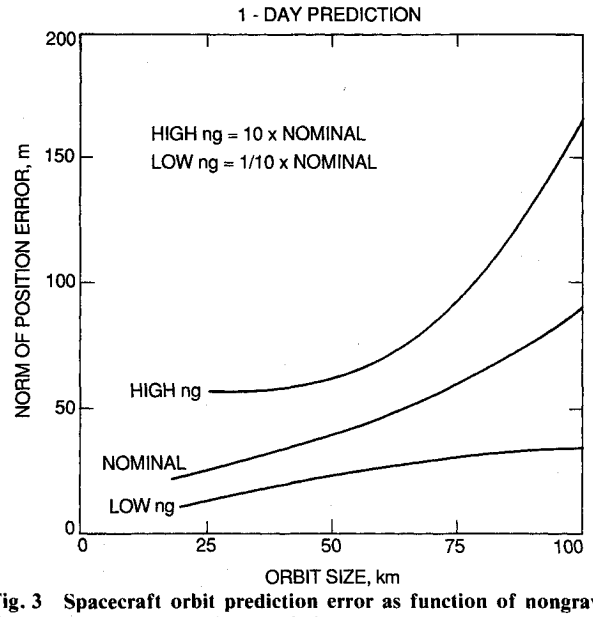

Fig. 3 Spacecraft orbit prediction error as function of nongravitational accelerations—1-day prediction.

The sensitivities of spacecraft 1-day orbit prediction error to Doppler and optical measurement errors are shown in Figs. 1 and 2, respectively, for a 20-km orbit. The norm of the position error is plotted as a function of the measurement error. Figure 1 shows that the orbit prediction error is relatively insensitive to the Doppler measurement error. The abscissa spans the range of Doppler measurement error from X-band frequencies to S-band frequencies. The insensitivity to Doppler measurement error indicates that the orbit determination error is dominated by other error sources, most notably the optical measurement error. Figure 2 shows a pronounced sensitivity to optical measurement error. The abscissa spans the range of optical measurement error from 1 to 40 m. This corresponds to a variation in the camera resolution error from several pixels to several hundred pixels. These results indicate that a substantial improvement in orbit determination accuracy is achievable if one-pixel landmark tracking can be achieved.

The sensitivity of spacecraft orbit prediction error to nongravitational accelerations is shown in Figs. 3 and 4 for 1-day and 9-day predictions, respectively. The norm of the spacecraft prediction error is shown for three levels of nongravitational accelerations as a function of orbit size. The high nongravitational (HIGH ng) case refers to multiplying the baseline a priori uncertainties in the constant and stochastic accelerations by a factor of 10, and the low nongravitational (LOW ng) case refers to dividing these same acceleration uncertainties by a factor of 10. These results indicate moderate sensitivity to nongravitational accelerations for short-term predictions, whereas long-term predictions are dominated by nongravitational accelerations.

Spacecraft orbit prediction accuracy is a function of our ability to determine the current state of the system as well as to characterize stochastic processes that may be driving the system. The system state includes spacecraft position and velocity, nucleus attitude, and other parameters such as gravity harmonic coefficients and moments of inertia. In this study, stochastic processes are included only in the nongravitational accelerations.

When dynamic stochastic processes are not important, the orbit prediction problem is relatively straightforward. Measurements are processed, and an estimate of the current state is obtained. A deterministic mapping is performed to the epoch of interest, and the orbit prediction error is determined principally by measurement errors. The situation is quite different when dynamic stochastic processes are driving the system. These stochastic nongravitational accelerations must be included in the mapping. As a result, long-term predictions are dominated by the stochastic accelerations. The long-term spacecraft orbit prediction cannot be significantly improved, in general, by processing more accurate data or introducing new data types. Improvements in accuracy are best obtained by shortening the prediction time.

A significant orbit prediction time is necessary to give the mission operations team time to plan science data gathering sequences and to command the spacecraft to execute these sequences. Science sequences may involve pointing instruments or deployment of a penetrator to the surface of the nucleus. The prediction time is measured from acquisition of the last data point, such as shuttering the camera for optical data, to implementation of science sequences and includes time to process data, generate orbit determination solutions, and generate spacecraft command sequences, as well as round-trip light time. During this time, the spacecraft orbit error resulting from nongravitational accelerations may grow to a level that is unacceptable for science observations or delivery of the penetrator. This would surely be the case if the HIGH nongravitational acceleration level shown in Figs. 3 and 4 were present, and the orbit prediction times were much longer than 1 day. One possible solution, with potentially significant cost and mass implications, would be to introduce a drag-free accelerometer as a navigation instrument to provide improved prediction (and possibly control) of spacecraft position.

Cometary Nucleus Attitude Prediction

Science observations and the delivery of a penetrator to the surface of the nucleus require estimates of the cometary nucleus attitude. The attitude and attitude error covariance may be mapped to various epochs that may be of interest for these purposes.

To obtain an estimate of the strength of Doppler data in determining the attitude of the nucleus, consider another simplified example. For a distant spacecraft in an equatorial circular orbit about a cometary nucleus, the acceleration component along the Earth-spacecraft line of sight including the perturbative acceleration of the C_{22} gravity harmonic may be approximated by

$$a = a_c - \sin i \sin(\omega_s t + \theta_s)\,[a_0 + a_1 \cos(2\omega_n t + \theta_n)] \qquad (4)$$

where

$$a_0 = \mu/r^2$$

$$a_1 = (9/2)\mu C_{22}(r_n^2/r^4)$$

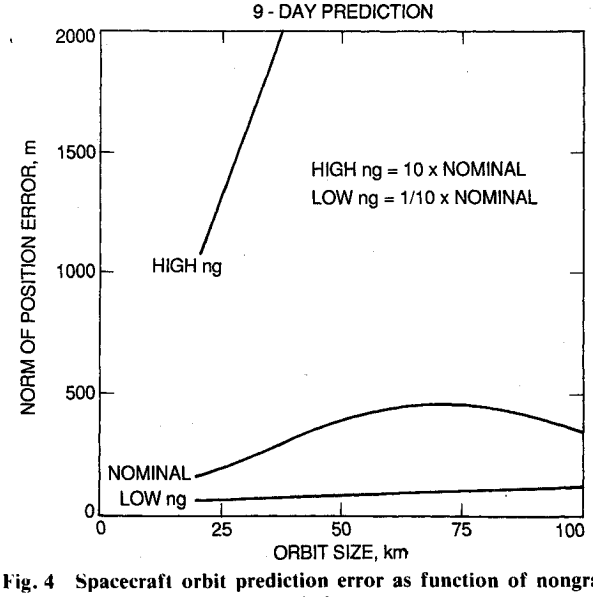

Fig. 4 Spacecraft orbit prediction error as function of nongravitational accelerations—9-day prediction.

Table 7 Cometary nucleus attitude estimation errors

Prediction epoch[a]	α, deg	δ, deg	θ, deg
20-km orbit			
0 days	0.048	0.032	0.105
1 day	0.048	0.033	0.111
9 days	0.049	0.032	0.174
50-km orbit			
0 days	0.108	0.062	0.237
1 day	0.092	0.063	0.238
9 days	0.091	0.063	0.533
100-km orbit			
0 days	0.179	0.230	0.154
1 day	0.281	0.180	0.328
9 days	0.360	0.086	0.384

[a]Time from last data point used in solution.

Table 8 Spacecraft science instrument pointing errors

Prediction epoch[a]	β, deg	γ, deg
20-km orbit		
0 days	0.023	0.018
1 day	0.060	0.019
9 days	0.424	0.030
50-km orbit		
0 days	0.023	0.019
1 day	0.040	0.019
9 days	0.442	0.041
100-km orbit		
0 days	0.013	0.016
1 day	0.021	0.023
9 days	0.080	0.017

[a]Time from last data point used in solution.

The line-of-sight acceleration component of the cometary nucleus relative to an Earth-based tracking station is given by a_c. The orbital rotation rate of the spacecraft about the cometary nucleus is given by ω_s, and i is the inclination of the orbit in the plane-of-the-sky coordinate system. The angle θ_s defines the spacecraft position relative to the nodal crossing at the initial time. The spin rate and prime meridian of the nucleus are given by ω_n and θ_n, respectively. The radius of the spacecraft orbit is r and the radius of the nucleus is r_n. The Doppler measurement is obtained by simply integrating the above acceleration over time.

The Doppler measurements are sampled at a rate Δt over the length of the data arc t_d. The covariance matrix of nucleus spin rate and prime meridian is obtained by integrating over the data arc to obtain the information matrix and inverting. If we assume that the nucleus gravity parameter μ and the spacecraft and cometary ephemerides are known, the covariance of the spin rate and prime meridian is approximated by

$$\begin{bmatrix} \sigma_\omega^2 & \rho\sigma_\omega\sigma_\theta \\ \rho\sigma_\omega\sigma_\theta & \sigma_\theta^2 \end{bmatrix} = \frac{192\omega_n^2\Delta t\sigma_\rho^2}{a_1^2\sin^2 i}\begin{bmatrix} 1/t_d^3 & -1/2t_d^2 \\ -1/2t_d^2 & 1/3t_d \end{bmatrix} \quad (5)$$

For a 20-km spacecraft orbit and 30-day data arc, this simplified analysis gives a spin rate error σ_ω of 1×10^{-7} deg/s and a prime meridian error σ_θ of 0.14 deg. These results are a bit optimistic and assume that optical data are available to aid in the determination of orbit parameters. The error in determining the attitude of the nucleus, based on optical data, may be approximated by assuming a landmark identification error of 20 m at the surface. The attitude determination error associated with optical imaging is therefore about 0.38 deg.

Cometary nucleus attitude estimation errors derived from a detailed covariance analysis are shown in Table 7 for orbits with periapsis radii of 20, 50, and 100 km. The attitude errors range from about 0.03 to 0.4 deg as given in terms of the pole and prime meridian. These values agree fairly well with the simplified analysis given previously even though they include many more error sources.

Science Instrument Pointing

For science instrument pointing, the location of a point on the surface of the nucleus relative to the spacecraft is of primary interest. The position error of a point on the surface may be approximated by simply scaling the nucleus attitude estimation errors given in Table 7 by the radius of the nucleus. Thus, the error in the position of a point on the surface of the nucleus in inertial space ranges from about 2 to 20 m. This position error may be combined directly with the spacecraft orbit prediction errors given in Table 6 to obtain an estimate of science instrument pointing errors.

The estimated science instrument pointing errors are given in Table 8 for the same three orbit cases discussed previously. These errors were obtained by combining the spacecraft orbit prediction errors given in Table 6 with the preceding attitude estimation errors neglecting correlations. The pointing angles are given for the downtrack (β) and crosstrack (γ) directions defined above. The current pointing accuracy requirement is around 0.05 deg (1 σ).

Estimation of Physical Parameters of Nucleus

The covariance analysis of spacecraft orbit prediction errors also includes evaluations of errors in the physical properties of the nucleus. These errors are given in Table 9 for spacecraft orbit periapsis radii of 20, 30, and 100 km. Also given in Table 9 are the nominal values of these parameters. The errors are given as percentages of nominal values or as absolute errors, whichever is more meaningful.

The axes of the nucleus are fixed with respect to two landmarks. Specification of latitude and longitude for the two landmarks is used to define the north pole and the prime meridian. Landmark location errors given in Table 9 are for the fourth landmark identified in Table 1. This landmark has Cartesian position coordinates $R_{\lambda x}$, $R_{\lambda y}$, and $R_{\lambda z}$. The relative landmark location errors indicate the accuracy with which surface features may be tied together on a map and potential penetrator landing sites identified.

The applied moment estimation errors vary from an order of magnitude to several orders of magnitude greater than the nominal values. These results indicate that during the quiescent phase of the nucleus, torques are at best barely detectable (and only about the spin axis). This situation may change as the nucleus approaches perihelion.

The mass of the nucleus may be determined with great precision. This result is not surprising since this parameter has the strongest signature in the Doppler data among the various physical parameters and is consistent with results obtained on other missions. For the same reason, the low-degree gravity harmonics may be estimated with moderate precision; however, this determination deteriorates rapidly for larger orbit sizes or for higher-degree harmonics.

The determination of the elements of the inertia tensor of the nucleus is critical to spacecraft orbit determination and prediction of the nucleus attitude. The moments of inertia about the principal axes are also of scientific interest since they provide some insight into the internal mass distribution. It is well known that the internal mass distribution and consequently the moments of inertia of the nucleus cannot be determined uniquely by external measurement of the gravity field. Also, the moments of inertia cannot be determined uniquely by observation of the tumbling of a free body in inertial space. However, the moments of inertia may be determined by combining observations of nucleus rotation with the gravity field determined by observations of spacecraft motion.

Both the gravity field and the inertia tensor may be obtained by integrating the density distribution over the volume of the

Table 9 Cometary nucleus parameter estimation errors

Parameters	Nominal values	Errors, 1σ Orbit size 20 km	30 km	100 km
Landmark locations, m		(absolute error)		
$R_{\lambda x}$	+2219	2.9	3.3	5.2
$R_{\lambda y}$	−2219	3.1	3.1	6.5
$R_{\lambda z}$	+2219	3.2	3.7	23.4
Moments of inertia, kg-m^2		(percent of nominal)		
I_{xx}	3.85×10^{20}	0.452	1.01	19.3
I_{yy}	7.69×10^{20}	0.436	0.93	13.7
I_{zz}	8.97×10^{20}	0.436	1.41	14.6
Applied moment, N-m		(absolute error)		
M_x	2.2×10^{5}	1×10^{10}	3×10^{10}	5×10^{10}
M_y	2.2×10^{5}	4×10^{9}	1×10^{10}	4×10^{10}
M_z	2.2×10^{5}	1×10^{6}	2×10^{6}	2×10^{6}
Mass, kg		(percent of nominal)		
m	1.13×10^{14}	0.037	0.027	0.072
Gravity harmonics		(absolute error)		
C_{20}	−0.500	0.00289	0.00246	0.20420
C_{21}	0	0.00092	0.00359	0.06968
C_{22}	+0.140	0.00034	0.00050	0.06978
S_{21}	0	0.00107	0.00498	0.06773
S_{22}	0	0.00043	0.00056	0.06936
C_{30}	0	0.06820	0.08269	0.97715
C_{31}	0	0.00216	0.00459	0.06758
C_{32}	0	0.00082	0.00277	0.00850
C_{33}	0	0.00065	0.00127	0.01688
S_{31}	0	0.00243	0.00561	0.00977
S_{32}	0	0.00017	0.00071	0.01292
S_{33}	0	0.00070	0.00136	0.02186

nucleus. The integrals that define the second-degree gravity harmonic coefficients are quite similar to the integrals that define the elements of the inertia tensor.[10] The following relationships are obtained by simply adding and subtracting the integrands that define these parameters and performing the same operations on both sides of the equations that define these parameters:

$$\begin{aligned} I_{xx} - I_{yy} &= -4mr_0^2C_{22} \\ I_{yy} - I_{zz} &= mr_0^2(C_{20} + 2C_{22}) \\ I_{zz} - I_{xx} &= -mr_0^2(C_{20} - 2C_{22}) \\ I_{xy} &= -2mr_0^2S_{22} \\ I_{yz} &= -mr_0^2S_{21} \\ I_{xz} &= -mr_0^2C_{21} \end{aligned} \tag{6}$$

where m is the mass of the nucleus and r_0 is its reference radius. These six equations place constraints on the relationship between the inertia tensor elements and gravity harmonics that link the gravity field determination to the rotational dynamics. However, only five of these equations are independent. The third equation may be obtained by adding the first two equations. Observe that there are six independent elements in the inertia tensor and five harmonic coefficients that are related to these elements. For this reason, it is not possible to completely describe the inertia tensor from gravity measurements. The differences in the moments of inertia may be determined, but the absolute moment of inertia about any axis cannot be determined. A single piece of information that would enable these parameters to be related is the moment of inertia about the origin or the trace of the inertia tensor. For that matter, knowledge of a nonzero moment of inertia about any axis would do.

Next, consider the rotational equations of motion[11] that relate the observed angular acceleration $\dot{\Omega}$ and body-fixed spin rates to the applied moment M.

$$\begin{aligned} M &= I\dot{\Omega} + \Omega \times H \\ H &= I\Omega \end{aligned} \tag{7}$$

The angular velocity vector Ω consists of the body-fixed rotation components ω_x, ω_y, and ω_z, and the inertia tensor is given by

$$I = \begin{bmatrix} I_{xx} & I_{xy} & I_{xz} \\ I_{xy} & I_{yy} & I_{yz} \\ I_{xz} & I_{yz} & I_{zz} \end{bmatrix}$$

If we rotate to a body-fixed coordinate system defined along the principal axes, the crossproducts of inertia vanish and Euler's equations are obtained:

$$\begin{aligned} M_x &= I_{xx}\dot{\omega}_x + (I_{zz} - I_{yy})\omega_y\omega_z \\ M_y &= I_{yy}\dot{\omega}_y + (I_{xx} - I_{zz})\omega_z\omega_x \\ M_z &= I_{zz}\dot{\omega}_z + (I_{yy} - I_{xx})\omega_x\omega_y \end{aligned} \tag{8}$$

Euler's equations may be rewritten as

$$\begin{aligned} I_{xx} &= \frac{M_x}{\dot{\omega}_x} - \frac{\omega_y\omega_z}{\dot{\omega}_x}(I_{zz} - I_{yy}) \\ I_{yy} &= \frac{M_y}{\dot{\omega}_y} - \frac{\omega_z\omega_x}{\dot{\omega}_y}(I_{xx} - I_{zz}) \\ I_{zz} &= \frac{M_z}{\dot{\omega}_z} - \frac{\omega_x\omega_y}{\dot{\omega}_z}(I_{yy} - I_{xx}) \end{aligned} \tag{9}$$

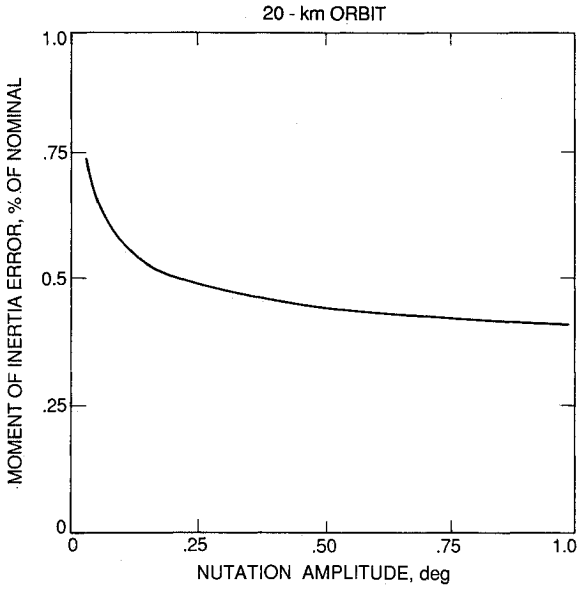

Fig. 5 Error in determining cometary nucleus moment of inertia as function of nutation angle.

The differences of inertia may be obtained directly from the second-order gravity harmonics as shown in Eq. (6). The spin rates and angular accelerations may be determined from direct observation of landmarks or the time-varying signature of gravity harmonics in the Doppler tracking data. Any substantial applied torques from outgassing or the solar gravity gradient can also be determined from their unique signatures. These individual pieces of information may be combined as indicated in Eq. (9) to obtain solutions for the moments of inertia.

The moment of inertia estimation errors given in Table 9 range from about 0.5% to 20% as the orbit size varies from 20 to 100 km. This growth may be directly attributed to the growth in the estimation error associated with the second-degree gravity harmonic coefficients. The moment of inertia estimation error is also influenced by the amount of nutation experienced by the nucleus. The greater the amount of nutation, the smaller these estimation errors become. For the case of rotation about a principal axis, the spin axis is fixed in inertial space (in the absence of external torques or outgassing), and the angular accelerations are zero. This makes the ratios of spin rates and applied moments to angular accelerations given in Euler's equations [Eq. (9)] indeterminate so that an estimate of moments of inertia cannot be obtained. The effect of nutation angle on the determination of moments of inertia is shown in Fig. 5. For the purpose of this illustration, the nutation angle is defined as the mean displacement of the cartographic north pole from the angular momentum vector direction. For nutation angles down to a tenth of a degree, the moments of inertia can be determined to less than 1% for a 20-km orbit.

Summary and Conclusions

This paper has described the orbit determination strategy and accuracy during portions of the postrendezvous phases of the Comet Rendezvous/Asteroid Flyby mission. During the postrendezvous phases, accurate orbit determination is needed to support trajectory control maneuvers, science instrument pointing, and deployment of a penetrator to the surface of the nucleus. A new development is the tracking of landmarks. This technique results in considerable improvement in orbit determination accuracy over simply tracking the center of figure. It is shown that short-term predictions of a day or so are dominated by measurement errors whereas long-term predictions of several days are dominated by nongravitational accelerations due to cometary outgassing, solar radiation pressure, and other effects. The orbit prediction errors grow from tens of meters to several hundred meters over nine days.

Spacecraft orbit determination errors are given for various orbit sizes ranging from 20 km to 1500 km. The results are dominated by optical measurement errors when the spacecraft is relatively close to the nucleus and increase as the size of the orbit is increased. For the orbit sizes of primary interest, ranging from 20 to about 100 km, the orbit determination errors vary from 10 to 50 m for a 1-day prediction and up to 400 m for a 9-day prediction. Results are also given for cometary nucleus attitude estimation and prediction. These results tend to follow the same trends as the spacecraft orbit determination results, and attitude estimation errors vary from 0.03 deg to 0.5 deg over the range of orbit sizes from 20 to 100 km. Estimation of the spacecraft orbit and cometary nucleus attitude results in the incidental determination of many parameters that describe the nucleus and are of interest for science, such as mass properties, dust and outgassing properties, and the gravity field.

Acknowledgments

The research described in this paper was carried out by the Jet Propulsion Laboratory, California Institute of Technology, under contract with NASA. The authors would like to thank V. Alwar, J. B. Jones, and D. Sonnabend for many helpful discussions.

References

[1]Draper, R. F., "The Comet Rendezvous Asteroid Flyby Project," 38th Congress of the International Astronautical Federation, Brighton, England, UK, IAF Paper 87-446, Oct. 1987.

[2]Miller, S. L., and Lisman, S., "Rendezvous with Comet Kopff," *Spaceflight,* Vol. 31, June 1989, pp. 195-201.

[3]Weeks, C. J., "Orbit Determination for the Mariner Mark II Comet Rendezvous/Asteroid Flyby Mission: The Orbiting Phase," *Advances in the Astronautical Sciences: Astrodynamics 1985,* Vol. 58, Pt. II, edited by B. Kaufman et al., Univelt, San Diego, 1986, pp. 1045-1064.

[4]Miller, J. K., and Wood, L. J., "Navigation of the Mariner Tempel 2 Mission: Orbit Phase and Penetrator Deployment," AIAA Paper 87-0092, Jan. 1987.

[5]Gombosi, T. I., "An Orbital Evolution Model of the Nucleus-Coma Interface Region of Comet P/Tempel-2," Space Physics Research Lab., Univ. of Michigan, Ann Arbor, MI, Preprint, March 1987.

[6]Hamilton, T. W., and Melbourne, W. G., "Information Content of a Single Pass of Doppler Data from a Distant Spacecraft," *The Deep Space Network Space Programs Summary 37-39,* Vol. III, Jet Propulsion Lab., Pasadena, CA, May 1966, pp. 18-23.

[7]Wood, L. J., "Orbit Determination Singularities in the Doppler Tracking of a Planetary Orbiter," *Journal of Guidance, Control, and Dynamics,* Vol. 9, No. 4, 1986, pp. 485-494.

[8]Bierman, G. J., *Factorization Methods for Discrete Sequential Estimation,* Academic, New York, 1977, pp. 171-178.

[9]Goldstein, H., *Classical Mechanics,* Addison Wesley, Reading, MA, 1980.

[10]Heiskanen, W. A., and Moritz, H., *Physical Geodesy,* W. H. Freeman, San Francisco, CA, 1967.

[11]Greenwood, D. T., *Principles of Dynamics,* Prentice-Hall, Inc., Englewood Cliffs, NJ, 1965.